ISSN 1063-7761, Journal of Experimental and Theoretical Physics, 2007, Vol. 105, No. 3, pp. 617–625. © Pleiades Publishing, Inc., 2007.
Original Russian Text © V.I. Zinenko, N.G. Zamkova, E.G. Maksimov, S.N. Sofronova, 2007, published in Zhurnal Éksperimental'noĭ i Teoreticheskoĭ Fiziki, 2007, Vol. 132, No. 3, pp. 702–711.

ORDER, DISORDER, AND PHASE TRANSITION IN CONDENSED SYSTEMS

Lattice Dynamics and Ferroelectric Instability in Ordered and Disordered $PbSc_{1/2}Ta_{1/2}O_3$ and $PbSc_{1/2}Nb_{1/2}O_3$ Solid Solutions

V. I. Zinenko[a], N. G. Zamkova[a], E. G. Maksimov[b], and S. N. Sofronova[a]

[a] *Kirensky Institute of Physics, Siberian Division, Russian Academy of Sciences, Krasnoyarsk, 660036 Russia*
[b] *Lebedev Physical Institute, Russian Academy of Sciences, Moscow, 119991 Russia*
e-mail: maksimov@lpi.ru

Received March 28, 2007

Abstract—The dynamic Born charges and the frequency spectra of lattice oscillations in the crystals of ordered and disordered $PbSc_{1/2}Ta_{1/2}O_3$ (PST) and $PbSc_{1/2}Nb_{1/2}O_3$ (PSN) solid solutions have been calculated within the framework of the generalized Gordon–Kim model with allowance for the dipole and quadrupole polarizabilities. The phonon spectra of both compounds contain ferroelectric soft modes. The influence of various interactions on the magnitude of dynamic charges and ferroelectric instability in PSN and PST solid solutions has been studied and it is shown that both these charges and the ferroelectric instability are determined by the competition between long-range dipole–dipole interactions and short-range dipole–charge interactions, the determining role played by the interaction of Nb (Ta) cations and oxygen anions in the Nb–O (Ta–O) bond direction.

PACS numbers: 61.50.Ah, 63.20.Dj, 71.15.Mb

DOI: 10.1134/S1063776107090191

1. INTRODUCTION

Among numerous ferroelectric materials, of special interest are lead scandium tantalate $PbSc_{1/2}Ta_{1/2}O_3$ (PST) and lead scandium niobate $PbSc_{1/2}Nb_{1/2}O_3$ (PSN) solid solutions possessing perovskite structures in a fully disordered phase. The physical properties and the character of phase transitions in these compounds depend on the degree of ordering of scandium and tantalum (niobium) ions. Disordered compounds exhibit a smeared ferroelectric phase transition with a relaxor character that depends on the degree of ordering, while the ordered PST (Pb_2ScTaO_6) and PSN (Pb_2ScNbO_6) behave as usual ferroelectric compounds (see [1–4] and references therein).

The high-temperature phases of disordered PSN and PST solid solutions have a $Pm3m$ symmetry (representing the structure of perovskites with the general chemical formula ABO_3), while the ordered solid solutions exhibit an $Fm3m$ symmetry (elpasolite structure). As the temperature decreases, both ordered and disordered solid solutions exhibit a ferroelectric phase transition to a rhombohedral phase. The symmetry of the low-temperature phase of PSN is $R3m$, while the symmetry of the low-temperature phase of PST has not yet been fully established [4–6].

Most of the experimental investigations were devoted to the structure and physical properties of PSN and PST solid solutions in the region of the ferroelectric phase transition. It was shown [7–9] that disordered phases of these solid solutions contain ordered nanodomains, the existence of which is confirmed by the results of experimental investigations of the crystal lattice dynamics, in particular, using the method of Raman scattering spectroscopy [8, 9]. Indeed, although Raman-active modes are symmetry-forbidden in the high-temperature phases of disordered solid solutions, the Raman spectra of ordered and disordered samples are nearly identical. The presence of such ordered nanodomains results in a more complicated pattern of crystal lattice distortions during the ferroelectric phase transition as compared to that in the ordered PSN and PST solid solutions. As was noted [7, 10], an important role in this phase transition is played both by the ferroelectric soft mode and by the antiferroelectric soft mode (in PSN) and the soft mode related to the rotation of oxygen octahedra (in PST). To the authors' knowledge, no theoretical calculations of the lattice dynamics of ordered and disordered PSN and PST solid solutions have been reported until now.

This paper presents the results of investigation of the lattice dynamics of the ordered and disordered PSN and PST solid solutions within the framework of the generalized Gordon–Kim model. Possible factors responsible for the ferroelectric instability in these compounds are discussed.

2. RESULTS AND DISCUSSION

We have calculated the frequency spectra of lattice oscillations, the dynamic Born charges, and the elastic moduli of the ordered and disordered PSN and PST solid solutions within the framework of the generalized Gordon–Kim model of an ionic crystal with allowance

Table 1. Lattice parameters (a_0) and elastic moduli (C_{ij}) of disordered and ordered PSN and PST solid solutions

Compound	a_0, Å	C_{11}, 10^2 GPa	C_{12}, 10^2 GPa	C_{44}, 10^2 GPa
Disordered				
$PbSc_{1/2}Nb_{1/2}O_3$	3.94	1.58	0.72	0.82
$PbSc_{1/2}Ta_{1/2}O_3$	4.03	2.09	0.74	0.75
Experiment				
$PbSc_{1/2}Ta_{1/2}O_3$ [21]		1.84	0.64	0.58
Ordered				
Pb_2ScNbO_6	7.88	1.64	0.74	0.86
Pb_2ScTaO_6	8.04	2.12	0.73	0.77

for the deformability and the dipole and quadrupole distortions of the electron density on ions [11]. In the case of disordered solid solutions, calculations were performed using the virtual crystal approximation [12]. The electron density on an individual ion and its self-energy in the Gordon–Kim model were calculated with allowance for the crystal field potential approximated by the Watson sphere. The crystal lattice parameters were determined through minimization of the total crystal energy. In the elpasolite structure, O^{-2} ions have a free coordinate that is related to their displacement along the Ta–O (Nb–O) bond. The positions of oxygen ions in the cubic phases of ordered solid solutions were also determined from the total energy minimum. In both PST and PSN, the oxygen octahedron is displaced by 0.08 Å toward Ta and Nb, respectively. Table 1 gives the calculated and experimental lattice parameters of completely ordered and disordered PSN and PST solid solutions. As can be seen, the calculated values coincide to within 3.5% with the experimental data. In addition, Table 1 gives the calculated and experimental values of elastic constants.

A characteristic feature of many oxides with ABO_3 perovskite structures is the anomalously large values of the dynamic Born charges on cations B and the components of the dynamic Born charge on oxygen anion $Z_{O_{||}}$ along the B–O bond [13]. However, according to the results of our calculations, the dynamic charges in tantalum compounds are rather small in comparison to those in other oxides (Table 2). In PST, the dynamic charge on Ta^{+5} is below the nominal value, while the dynamic charge on Nb^{+5} in the isomorphous niobate is close to the charges on cations B in oxides with perovskite structures. This tendency to a decrease in the dynamic charge with increasing atomic number of the cation has been also observed in pure ABO_3 perovskites [14].

In the model of polarizable ions [14], the high-frequency dielectric constant and the dynamic charges on ions in cubic crystals can be expressed as [10, 15]

$$\varepsilon_\infty = I + \frac{4\pi}{\Omega}\alpha_{\text{eff}}\left(I - \frac{4\pi}{3\Omega}\alpha_{\text{eff}}\right)^{-1}, \quad (1)$$

$$Z_{\text{din}}(i) = \frac{\varepsilon_\infty + 2}{3}Z_{\text{eff}}(i), \quad (2)$$

where $Z_{\text{eff}}(i)$ and α_{eff} are the effective charge and the effective polarizability of ions in the crystal. These effective quantities are determined by the short-range interactions as

$$\alpha^{\alpha\beta}_{\text{eff},\,ij} = \alpha_j[\delta_{\alpha\beta} + \alpha_i(\gamma^{\alpha\beta}_{ij} + \Gamma^{\alpha\beta}_{ij})]^{-1}, \quad (3)$$

$$Z^{\alpha\beta}_{\text{eff}}(i) = Z_{\text{ion}}(i)\delta_{\alpha\beta} - \sum_{j,\gamma}\alpha^{\alpha\gamma}_{\text{eff},\,ij}\left(T^{\gamma\beta}_{ji} - \left(\frac{4\pi}{3\Omega}\delta_{\gamma\beta} - \gamma^{\gamma\beta}_{ji}\right)Z_{\text{ion}}(j)\right), \quad (4)$$

where γ characterizes the difference between the internal field on the ion and the Lorentz field, describing the intercell interaction, and the Γ and T matrices describe the short-range interactions between the extended dipoles and the dipoles and charges, respectively.

For the ABO_3 perovskite structure, the values of non-Lorentzian structural constants $\gamma^{\gamma\beta}_{ij}$ for oxygen ions occupying tetragonal positions are nonzero, being especially large in the B–O bond direction. These very components of the $\gamma^{\gamma\beta}_{ij}$ tensor account for an increase in the effective polarizability σ_{eff} of oxygen ions in the

Table 2. Dynamic charges Z_{dyn} (in e units) and high-frequency permittivities ε_∞ of disordered and ordered PSN and PST solid solutions

Disordered	Z_{dyn}(Pb)	$Z_{\text{dyn}}(\langle\text{ScNb(Ta)}\rangle)$		$Z_{\text{dyn},\,||}$(O)	$Z_{\text{dyn},\,\perp}$(O)	ε_∞
$PbSc_{1/2}Nb_{1/2}O_3$	2.93	5.60		–4.71	–1.90	4.47
$PbSc_{1/2}Ta_{1/2}O_3$	2.81	4.41		–3.07	–2.07	4.18
Ordered	Z_{dyn}(Pb)	Z_{dyn}(Sc)	Z_{dyn}(Nb(Ta))	$Z_{\text{dyn},\,||}$(O)	$Z_{\text{dyn},\,\perp}$(O)	ε_∞
Pb_2ScNbO_6	2.99	4.76	6.44	–4.82	–1.89	3.86
Pb_2ScTaO_6	2.83	4.03	4.36	–2.70	–2.16	3.56

Table 3. Dynamic charges (in e units) on ion B [$Z_{dyn}(B)$] and oxygen [$Z_{dyn,\parallel}(O)$] in disordered and ordered PSN and PST solid solutions calculated with allowance for various interactions

	$\gamma = 0; \Gamma = 0; T = 0$		$\gamma \neq 0; \Gamma = 0; T = 0$		$\gamma \neq 0; \Gamma \neq 0; T = 0$		$\gamma \neq 0; \Gamma \neq 0; T \neq 0$		$\gamma \neq 0; \Gamma \neq 0; T \neq 0$ $T_{B-O_\parallel} = 0$	
	ordered	disordered	ordered	disordered	ordered	disordered	ordered	disordered	ordered	disordered
PSN	$\varepsilon_\infty = 3.23$	3.53	$\varepsilon_\infty = 3.24$	3.55	$\varepsilon_\infty = 3.86$	4.47	$\varepsilon_\infty = 3.86$	4.47	$\varepsilon_\infty = 3.86$	4.47
Nb/⟨B⟩	8.72	7.38	9.67	8.11	12.19	10.71	6.14	5.60	15.47	13.45
$O_\parallel$	–3.49	–3.69	–7.83	–8.36	–10.16	–11.55	–4.32	–4.71	–8.99	–12.57
PST	$\varepsilon_\infty = 3.10$	3.41	$\varepsilon_\infty = 3.11$	3.42	$\varepsilon_\infty = 3.56$	4.18	$\varepsilon_\infty = 3.56$	4.18	$\varepsilon_\infty = 3.56$	4.18
Ta/⟨B⟩	8.51	7.22	8.83	7.77	10.19	9.75	4.36	4.41	13.91	12.78
$O_\parallel$	–3.40	–3.61	–7.08	–8.06	–8.50	–10.58	–2.70	–3.07	–7.47	–11.44
PST*	$\varepsilon_\infty = 3.43$	3.48	$\varepsilon_\infty = 3.45$	3.50	$\varepsilon_\infty = 4.37$	4.46	$\varepsilon_\infty = 4.37$	4.46	$\varepsilon_\infty = 4.37$	4.46
Ta*/⟨B⟩	9.05	7.30	10.44	8.41	14.88	11.70	5.07	5.20	20.03	14.88
$O_\parallel$	–3.62	–3.65	–8.67	–8.69	–12.53	–12.49	–3.56	–4.01	–11.04	–13.69

B–O bond direction and for the appearance of anomalously large values of the dynamic charges [11, 15] in perovskite structures, including PSN and PST solid solutions. This is illustrated by the data in Table 3, which shows contributions to the dynamic charges calculated using Eqs. (1)–(4) for Nb, Ta, and $O_\parallel$ ions (for brevity, contributions to the dynamic charge on lead and the oxygen charge component $Z_{O_\perp}$ are omitted). Allowance for the long-range dipole–dipole interaction leads to a still greater anisotropy in $\hat{\alpha}_{eff}$ of oxygen ions and to an increase in the dynamic Born charge (Table 3, third column 3). At the same time, the short-range interaction between extended dipoles and the spherically distributed charge density significantly decreases the dynamic charges (Table 3, fourth column). The results of our calculations showed that this decrease in the dynamic charges on metal ions at the center of the octahedron and in the oxygen ion charge components in the B–O bond direction is related predominantly to the interaction between the extended oxygen ion dipoles and the spherically distributed charge density on ion B, while the dielectric constant (1) is independent of this interaction. Table 3 (fifth column) also shows the dynamic charges calculated with neglect of only the short-range interaction between the extended oxygen ion dipole and the extended charge on Nb and Ta (T_{B-O} element of the **T** matrix). As can be seen from a comparison of the third and fifth columns in Table 3, the absence of this single interaction even leads to a very small increase in the dynamic charge on ion B as compared to the case of the total absence of short-range dipole–charge interactions. The results of our calculations showed that this behavior is related to the fact that the short-range interaction between the extended charge on ion B and extended dipoles $O_\perp$ increases the dynamic charge on ion B (although this interaction is much smaller in magnitude).

It should be noted that the dynamic charge is also influenced by the polarizability of a metal ion. Table 3 shows the values of dynamic Born charges calculated for a PST* solid solution with excited Ta^{*+5} ions, which possess the outer electron shell configuration $5s^25p^64f^45d^{10}$ (instead of $5s^25p^64f^{14}$ in unexcited Ta^{+5} ion). Although the polarizability of the excited ion Ta^{*+5} is more than three times that of the unexcited one, the contribution of the short-range part of the charge–dipole interactions to the effective charge (4) also exhibits a significant (almost twofold) increase. As a result, the joint action of these two factors leads to a quite small increase in the dynamic charge.

Thus, the dynamic charge is determined by the rather fine balance between the competitive long-range dipole–dipole interactions and short-range dipole–charge interactions. A similar balance of these competitive interactions also determined the instability of oxides with perovskite structures with respect to the polar transverse mode of crystal lattice oscillations. Figures 1 and 2 show the total phonon spectra calculated for the disordered and ordered PSN and PST solid solutions with the lattice parameters determined in experiments. Table 4 presents the values of frequencies at the center of the Brillouin zone and at the point $R = \frac{2\pi}{a_0}\left(\frac{1}{2}\,\frac{1}{2}\,\frac{1}{2}\right)$. As can be seen, the difference between the frequencies of the crystal lattice oscillations in the ordered and disordered solid solutions is rather small. This similarity was also observed in experiments [8, 9].

A comparison of the data presented in Tables 2 and 4 shows that, despite the difference in the dynamic charges of pentavalent metal cations in PSN and PST

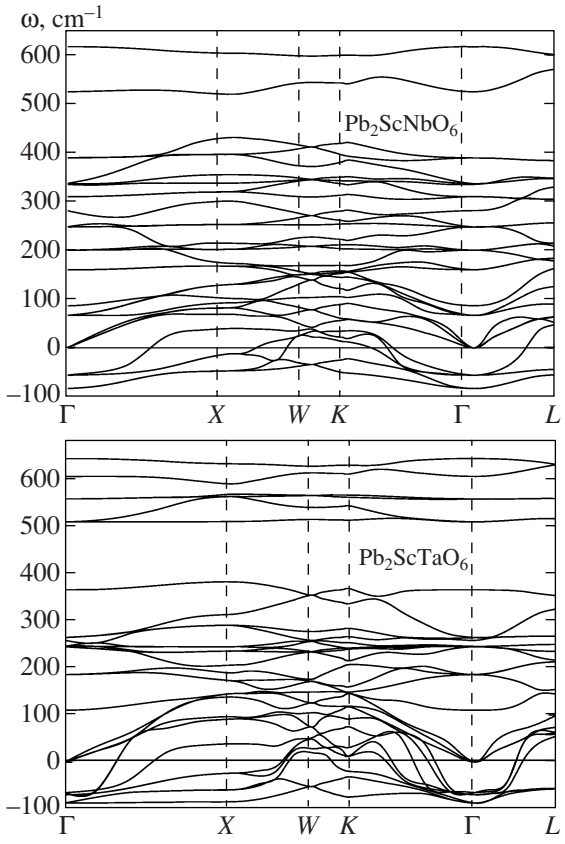

Fig. 1. Phonon spectra calculated for the ordered PSN and PST solid solutions (negative values refer to imaginary frequencies).

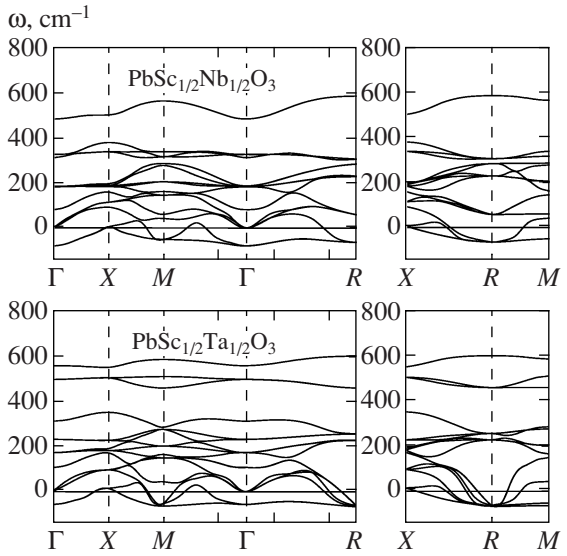

Fig. 2. Phonon spectra calculated for the disordered PSN and PST solid solutions (negative values refer to imaginary frequencies).

solid solutions, both ordered and disordered compounds are unstable with respect to the ferroelectric oscillation mode. Let us consider the case of disordered compounds (i.e., the perovskite structure) in more detail. Apparently, the most commonly accepted mechanism of the ferroelectric instability in oxides with the perovskite structure is the dipolar mechanism, which is based on the concept of long-range dipole–dipole interactions. This mechanism has been repeatedly discussed both within the framework of various empirical models of ionic crystals with polarizable ions (see, e.g., review [15] and references therein) and in quantum-mechanical calculations of the properties of oxides with perovskite structures [11, 13, 16–18]. Note, however, that an alternative mechanism of instability in the cubic perovskite structure has been also considered, which is based on the notion of several equiprobable equilibrium positions for ion B in the cubic ABO_3 phase [19]. The ab initio (first principles) calculations of Kvyatkovskii [16–18] have confirmed that the intercell long-range dipole–dipole interaction decreases the frequencies of the polar modes of lattice oscillations and may cause instability of the crystal. In particular, the quantum-mechanical cluster calculations of the contributions from long-range dipole–dipole interactions and short-range dipole–charge interactions to the diagonal elements of the force matrix of perovskite compounds showed that (i) the former contribution in oxides is anomalously large as compared to those in normal dielectrics and (ii) the minimum energy in the cubic phase calculated with neglect of this long-range interaction corresponds to the central position of ion B [18].

The long-range dipole–dipole contribution to the diagonal elements of the force matrix of cubic perovskites can be written as [18]

$$k_{dd}^{ii} = -\frac{4\pi e^2 Z_{\text{din}}^2(i)}{\Omega}\frac{}{\varepsilon_\infty + 2}. \qquad (5)$$

Table 5 presents the long-range dipole–dipole contributions (k_{dd}^{ii}) calculated using this formula in comparison to the short-range contributions (k_{sh}^{ii}). The latter values were determined by subtracting k_{dd}^{ii} from the total diagonal element of the force matrix calculated within the framework of the adopted approach. The first two columns in Table 5 show the low-energy (soft) polar mode determined with allowance for all interactions in the crystal and with neglect of the long-range dipole–dipole interaction (k_{dd}^{ij}), respectively. For comparison, this table also gives the aforementioned values for some other oxides with the perovskite structure. As can be seen from these data, the polarized dipole–dipole interactions determine the ferroelectric instability of the cubic phase in perovskite oxides: in the absence of this interaction, all compounds become stable with respect to the polar mode (third column in Table 5). These data also well agree with the results of ab initio calculations

Table 4. Lattice oscillation frequencies (cm^{-1}) for ordered (at $q = 0$) and disordered (at $q = 0$ and $q = R$) PSN and PST solid solutions (figures in parentheses indicate mode degeneracy)

Disordered (perovskite structure)			Ordered (elpasolite structure)			
	PSN	PST		PSN	PST	Experiment PST [8]
$q = 0$			$q = 0$			
$T_{1u}(2)$ TO	80.2i	56.9i	$T_{1u}(2)$ TO	83.0i	69.3i	
$T_{1u}(1)$ LO	80.9	107.9	$T_{1u}(1)$ LO	86.3	110.1	
$T_{2u}(3)$	182.3	173.6	$T_{2u}(3)$	200.1	185.7	
$T_{1u}(2)$ TO	186.2	232.9	$T_{1u}(2)$ TO	160.2	245.4	
$T_{1u}(1)$ LO	312.1	313.8	$T_{1u}(1)$ LO	281.0	258.2	
$T_{1u}(2)$ TO	326.7	499.4	$T_{1u}(2)$ TO	389.1	558.1	
$T_{1u}(1)$ LO	483.8	560.2	$T_{1u}(1)$ LO	524.5	605.7	
$q = R$			$q = R$			
$R_{15}(3)$	65.1i	62.6i	$T_{2g}(3)$	55.8i	64.7i	50
$R_{25}(3)$	57.4	67.3i	$T_{1g}(3)$	66.5	86.7i	
$R_{15}(3)$	228.5	228.4	$T_{2g}(3)$	247.7	244.7	370
$R_{25'}(3)$	305.4	256.8	$T_{1u}(2)$ TO	309.6	264.1	
			$T_{1u}(1)$ LO	334.8	365.3	
$R_{12'}(2)$	283.7	460.8	$E_g(2)$	336.3	509.5	500
$R_{2'}(1)$	585.9	602.8	$A_{1g}(1)$	616.9	643.5	740

Table 5. Low-energy polar mode frequencies (ω, cm^{-1}) and the contributions due to long-range dipole–dipole (k_{dd}) and short-range (k_{sh}) interactions to the diagonal elements of the force matrix of perovskite compounds (in the units of $4\pi e^2/\Omega$)

	ω	ω_{sh}	A		B		$O_{\parallel}$		$O_{\perp}$	
			k_{dd}	k_{sh}	k_{dd}	k_{sh}	k_{dd}	k_{sh}	k_{dd}	k_{sh}
$BaTiO_3$	–96	142	–1.36	3.75	–5.05	8.56	–4.77	6.23	–0.37	1.86
$BaZrO_3$	25	116	–1.26	3.68	–4.97	14.21	–3.99	10.82	–0.46	1.61
$PbTiO_3$	–77	127	–1.22	3.92	–4.72	8.49	–4.01	5.88	–0.42	1.46
$PbZrO_3$	–67	96	–3.40	3.01	–4.80	14.0	–3.15	9.80	–0.60	1.54
$SrTiO_3$	68	160	–1.14	3.31	–5.59	9.95	–4.76	8.18	–0.40	1.74
$KNbO_3$	–298	113	–0.29	1.88	–8.16	8.79	–5.98	3.73	–0.23	2.37
$KTaO_3$	129	147	–0.30	1.90	–3.51	19.43	–1.24	14.36	–0.43	2.65
$PbSc_{1/2}Nb_{1/2}O_3$	–80	76	–1.31	2.76	–4.86	10.02	–3.40	6.40	–0.54	1.88
$PbSc_{1/2}Ta_{1/2}O_3$	–57	96	–1.27	2.76	–3.12	14.82	–1.52	10.56	–0.69	2.98

for finite clusters [18]. However, a simple comparison of the short-range and long-range contributions to the force matrix elements does not allow one to judge the ferroelectric instability in a particular compound. Indeed, for example, these contributions are approximately equal in $BaTiO_3$ and $SrTiO_3$, but the latter compound is not ferroelectric under normal conditions. On the other hand, the short-range contributions for B and

Table 6. Square frequencies of the low-energy polar mode and C_0/C_1 frequencies (in $4\pi e^2/\Omega$ units)

	ω^2_{sh}	$-C_{0,\,sh}/C_{1,\,sh}$	ω^2	$-C_0/C_1$
$BaTiO_3$	1.08	0.72	−0.31	−0.48
$BaZrO_3$	1.01	0.61	0.034	0.028
$PbTiO_3$	0.80	0.58	−0.23	−0.31
$PbZrO_3$	0.75	0.58	−0.29	−0.33
$SrTiO_3$	1.13	0.75	0.16	0.15
$KNbO_3$	0.53	0.40	–2.97	–3.05
$KTaO_3$	1.04	0.77	0.69	0.55
$PbSc_{1/2}Nb_{1/2}O_3$	0.48	−0.40	−0.41	−0.64
$PbSc_{1/2}Ta_{1/2}O_3$	0.62	0.73	−0.25	−0.27

$O_\parallel$ ions in PSN and PST are significantly different, but both compounds exhibit the ferroelectric phase transition.

The long-range and short-range contributions to the low-energy polar mode frequencies cannot be separated in the general form (in contrast to the case of a diatomic crystal). These contributions can be separated only in elements of the dynamic matrix. Information concerning the role of various interactions in the ferroelectric instability is lost upon numerical diagonalization of the dynamic matrix. However, the perovskite structure also admits the analytical diagonalization of the dynamic (or force) matrix. In this case, triply degenerate (with neglect of the macroscopic field) frequencies of the optical polar modes are the roots of the cubic equation

$$(\omega^2)^3 + C_2(\omega^2)^2 + C_1\omega^2 + C_0 = 0. \quad (6)$$

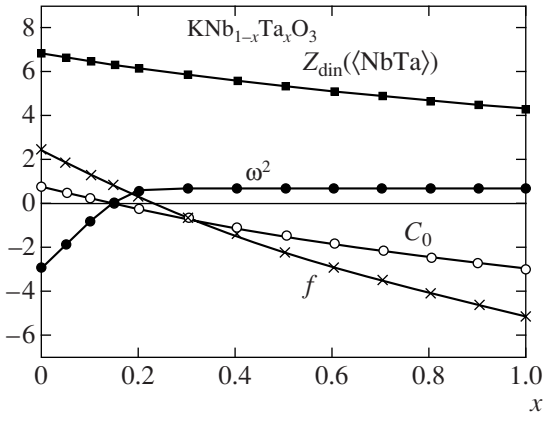

Fig. 3. Plots of (■) the dynamic charge on average ion, (×) force matrix element $f = D^{xx}_{B-O_\parallel}$, (○) C_0 coefficient, and (●) square frequency of the low-energy polar mode versus tantalum concentration x in $KNb_{1-x}Ta_xO_3$ (KNT) solid solutions (in $4\pi e^2/\Omega$ units).

The quantity ω^2 can be estimated in the first-order approximation with respect to C_0. In cases where the coefficient C_1 at the first-order term in the cubic equation is positive (which is valid for all compounds listed in Table 5, except $KNbO_3$), the square frequency of the low-energy polar mode is determined by the root of this equation, for which (in the first order)

$$\omega^2 \approx -C_0/C_1. \quad (7)$$

The sign of the square frequency is determined by the sign of C_0, the free term in cubic equation (7), which, in turn, is determined by a combination of the elements of the force (or dynamic) matrix $D^{\alpha\beta}_{ij}(q = 0)$ calculated with neglect of the macroscopic field. Our calculations showed that

$$C_0 = 5(cdf + 2cdg + cfg + 2dfg + b(c + f)(d + g) + (c + 2d)(f + 2g)j + b(c + 2d + f + 2g)j) \quad (8)$$

and

$$b = D^{xx}_{A-B}, \quad c = D^{xx}_{A-O_\parallel}, \quad d = D^{xx}_{A-O_\perp}, \quad f = D^{xx}_{B-O_\parallel}, \quad g = D^{xx}_{B-O_\perp}, \quad j = D^{xx}_{O_\parallel - O_\perp}. \quad (9)$$

For a negative C_1 (which corresponds, e.g., to $KNbO_3$), the square frequency of the low-energy polar mode is determined by the other root of the cubic sign of the square frequency and has a more complicated expression than (7), but the sign of the square frequency is still determined by the sign of C_0.

Table 6 (fifth and fourth columns) presents the values of the C_0/C_1 ratio and the square frequency of the low-energy polar mode in cubic perovskites. The third column in this table gives the values of $C_{0,\,sh}/C_{1,\,sh}$ calculated with neglect of the long-range dipole–dipole interactions (in which case the coefficient C_0 is always negative), and the second column gives the corresponding square frequencies. When the long-range dipole–dipole interaction is switched on, some compounds become ferroelectrically unstable (see the fourth column) and their coefficients C_0 become positive.

The magnitude and the sign of the square frequency of the low-energy polar mode depends nearly on all interactions in the crystal, but the most important role determining the existence of the ferroelectric instability is played by the competition between the long-range dipole–dipole interactions and the short-range dipole–charge interaction of ion B with the extended oxygen dipole along the B–O bond. This situation is clearly illustrated for $KTa_xNb_{1-x}O_3$ (KTN), in which the dynamic charges and optical spectra of lattice oscillations were calculated within the framework of the generalized Gordon–Kim model [11] for various x values and the experimental lattice parameter $a_0 = 4.0$ Å. Figure 3 shows the dependence of the square frequency of the low-energy polar mode ω^2 on the tantalum concentration x in KTN. It should be emphasized that the con-

Table 7. Eigenvectors of the ferroelectric mode and spontaneous polarizations P_s [C/m^2] in rhombohedral phases of disordered and ordered PSN and PST solid solutions

Disordered (perovskite structure)						
	Pb	⟨ScNb(Ta)⟩	$O_\perp$	$O_\parallel$	P_s (calcd.)	P_s (exp.)
$PbSc_{1/2}Nb_{1/2}O_3$	0.76	0.23	−0.42	−0.16	0.21	0.25 [23]
$PbSc_{1/2}Ta_{1/2}O_3$	0.75	0.15	−0.47	0.05	0.30	0.21 [22]

Ordered (elpasolite structure)							
	Pb	Nb(Ta)	Sc	$O_\perp$	$O_\parallel$	P_s (calcd.)	P_s (exp.)
Pb_2ScNbO_6	0.53	0.07	0.27	−0.29	−0.11	0.18	0.25
Pb_2ScTaO_6	0.54	0.04	0.11	−0.31	0.00	0.17	0.21

centration dependence of the soft mode frequency and the disappearance of the ferroelectric phase transition at small tantalum concentrations in KTN solid solutions are only obtained as a result of these calculations and not observed in experiment. Nevertheless, we present this result in order to demonstrate the importance of the B–O interaction in the mechanism of ferroelectric instability in perovskite oxides. Indeed, as Ta is added to $KNbO_3$, the most significant change is observed in the $f = D^{xx}_{B-O_\parallel}$ element of the force matrix, while the other elements are almost independent of the tantalum content (in the region of small dopant concentrations).

Figure 3 also shows the plots of $Z_{din}(B)$, C_0 from expression (8), and the force matrix element versus x. As can be seen, a change in the B–O interaction with the addition of tantalum is manifested by the strong dependence of C_0 on x, which leads to a sharp initial change in ω^2. At $x \approx 0.12$, both C_0 and ω^2 change sign and the KTN solid solution becomes stable with respect to the ferroelectric oscillation mode. It should be also noted that the real behavior of KTN with small tantalum concentrations is determined by the presence of the aforementioned ordered nanodomains. The virtual crystal approximation used above is evidently inapplicable to the description of such domains. Unfortunately, a theory taking into account the existence of nanodomains has not been developed so far.

Now let us return to the consideration of PST and PSN solid solutions. In the eigenvectors of the ferroelectric mode calculated for a series of perovskite compounds (Table 7), the main role is played by the displacements of lead and oxygen ions in the directions perpendicular to the Ta–O (Nb–O) bond, while the displacements of oxygen along the Ta–O (Nb–O) bond toward Ta (Nb) ions are insignificant. Experimental investigations of the structure of ferroelectric phases in PST and PSN solid solutions show that the maximum displacements from positions in the high-temperature phase of both ordered and disordered compositions are observed for Pb ions [6, 20]. When these ions are displaced along the eigenvector of the soft ferroelectric mode in the cubic perovskite phase, the energetically most favorable structures in both ordered and disordered PST and PSN solid solutions are those with displacements in the (111) directions. The symmetry of the crystal becomes rhombohedral (for the same number of atoms per unit cell), which agrees with the experimental situation [6, 20]. Table 7 presents the values of spontaneous polarization P_s calculated for the ions displaced along the eigenvector of the soft ferroelectric mode in the rhombohedral phase. Our results qualitatively agree with experiment [22, 23], although the calculated values are somewhat smaller than the measured ones.

In addition to the soft ferroelectric mode (T_{1u} symmetry), both ordered and disordered PST solid solutions exhibit two other types of instability, with T_{1g} (R_{25}) and T_{2g} (R_{15}) symmetry. The lowest mode is that of T_{1g} (R_{25}) symmetry, the eigenvectors of which correspond to rotations of the TaO_6 octahedron. As the rotation angle grows, the frequency of the ferroelectric mode increases, whereas the spontaneous polarization decreases. Figure 4 shows the dependences of the ferroelectric mode frequency and the spontaneous polarization on the small angle of rotation of the octahedron in the cubic phase. In addition, we have also calculated the total energy of the crystal and the Coulomb interaction, short-range interaction, and polarization energy contributions as functions of the octahedron rotation angle. As can be seen, the rate of growth of the Coulomb energy and the polarization energy exceeds the rate of the short-range drop in energy; this balance stabilizes the ferroelectric mode. Dmowski et al. [10] showed that crystal lattice distortions corresponding to rotations of the octahedron are present, in addition to ferroelectric distortions, in the rhombohedral phase of the PST solid solution.

The branch of crystal lattice oscillations related to rotations of the NbO_6 octahedron in PSN compounds is stable, in contrast to the case of PST solid solutions.

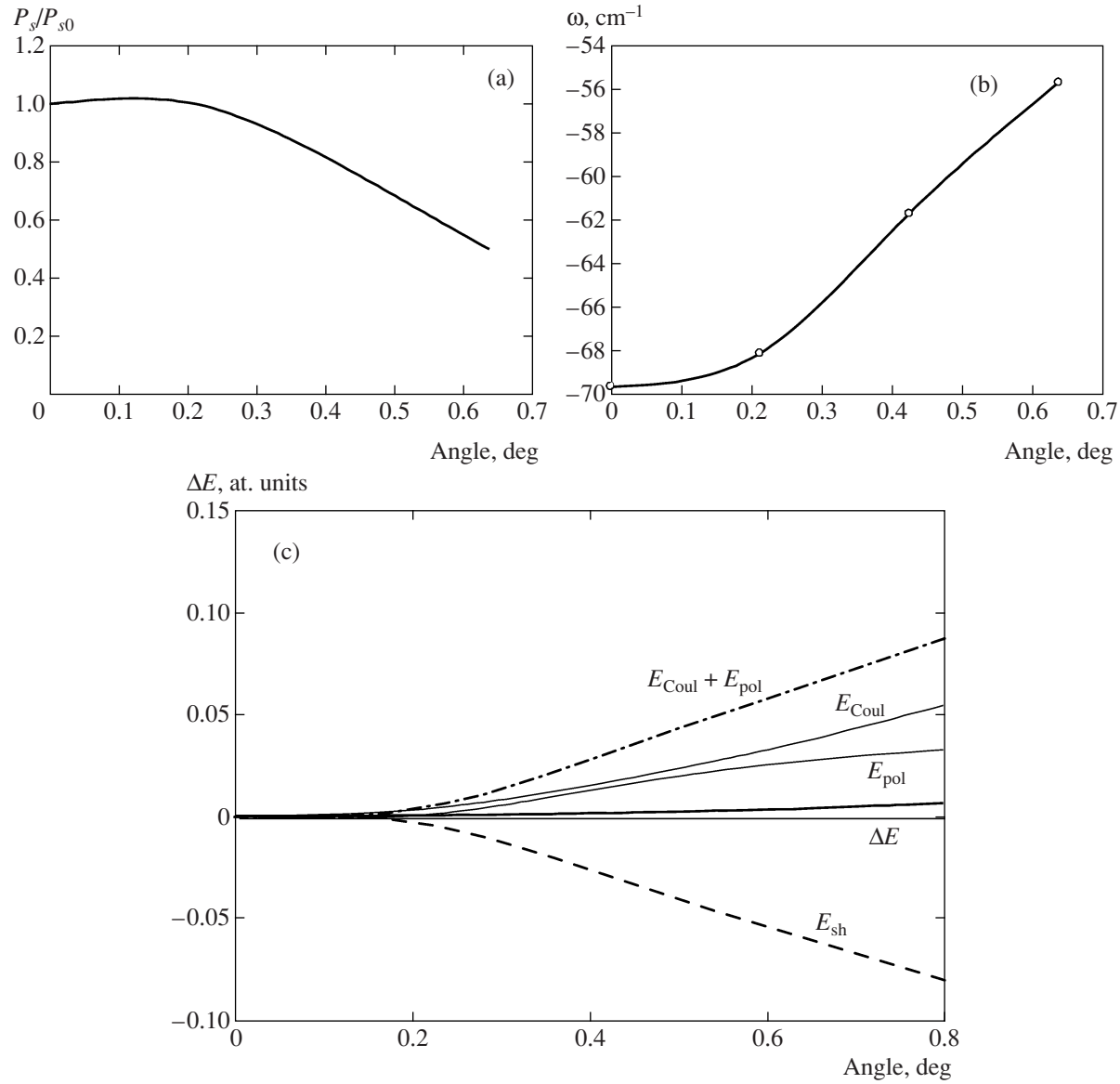

Fig. 4. Plots of (a) the spontaneous polarization, (b) the ferroelectric mode frequency, and (c) the total energy (ΔE) and contributions due to various interactions versus angle of rotation (deg) of the oxygen octahedron in the ordered PST solid solution.

Both ordered and disordered PSN solid solutions exhibit, in addition to ferroelectric instability, an antiferroelectric soft mode (Table 4, Figs. 1 and 2). The presence of two soft modes at various points of the Brillouin zone in disordered PSN solid solutions was experimentally confirmed [2, 7].

3. CONCLUSIONS

The frequency spectra of lattice oscillations, high-frequency permittivities, dynamic Born charges, and elastic moduli of ordered and disordered PSN and PST solid solutions have been calculated within the framework of the generalized Gordon–Kim model with allowance for the dipole and quadrupole polarizabilities. Both systems exhibit crystal lattice instability of several types, including ferroelectric instability. The dynamic charges and the ferroelectric instability in compounds with perovskite structures are determined by the competition between long-range dipole–dipole interactions and short-range dipole–charge interactions. All types of instability in PSN and PST solid solutions are characterized by close energies, which probably accounts for the rather complicated pattern of crystal lattice distortions in the low-temperature phase.

ACKNOWLEDGMENTS

The authors are grateful to O.E. Kvyatkovskii for fruitful discussions.

This study was supported in part by the Russian Foundation for Basic Research (project nos. 06-02-16091, 05-02-17359) and the Presidential Program of Support for Leading Scientific Schools in Russia.

REFERENCES

1. L. E. Cross, Ferroelectrics **76**, 241 (1987).
2. N. Takesue, Y. Fujii, M. Ichihara, and H. Chen, Phys. Rev. Lett. **82**, 3709 (1999).
3. C. Perrin, N. Menguy, O. Bidault, et al., J. Phys.: Condens. Matter **13**, 10231 (2001).
4. V. A. Isupov, Ferroelectrics **289**, 131 (2003).
5. B. Mihailova, U. Bismayer, B. Güttler, et al., J. Phys.: Condens. Matter **14**, 1091 (2002).
6. P. M. Woodward and K. Z. Baba-Kishi, J. Appl. Crystallogr. **35**, 233 (2002).
7. V. V. Laguta, M. D. Glinchuk, I. P. Bykov, et al., Phys. Rev. B **69**, 054103 (2004).
8. I. G. Siny, S. G. Lushnikov, and R. S. Katiyar, Ferroelectrics **231**, 115 (1999).
9. E. A. Rogacheva, Physica B (Amsterdam) **291**, 359 (2000).
10. W. Dmowski, M. K. Akbas, P. K. Davies, and T. Egami, J. Phys. Chem. Solids **61**, 229 (2000).
11. E. G. Maksimov, V. I. Zinenko, and N. G. Zamkova, Usp. Fiz. Nauk **174**, 1145 (2004).
12. V. I. Zinenko and S. N. Sofronova, Fiz. Tverd. Tela (St. Petersburg) **46**, 1252 (2004) [Phys. Solid State **46**, 1291 (2004)].
13. W. Zhong, R. D. King-Smith, and D. Vanderbilt, Phys. Rev. Lett. **72**, 3618 (1994).
14. N. G. Zamkova, V. I. Zinenko, O. V. Ivanov, et al., Ferroelectrics **283**, 49 (2003).
15. O. E. Kvyatkovskiĭ and E. G. Maksimov, Usp. Fiz. Nauk **154**, 3 (1988) [Sov. Phys. Usp. **31**, 1 (1988)].
16. O. E. Kvyatkovskiĭ, Fiz. Tverd. Tela (Leningrad) **27**, 2673 (1985) [Sov. Phys. Solid State **27**, 1603 (1985)].
17. O. E. Kvyatkovskii, Ferroelectrics **153**, 201 (1994).
18. O. E. Kvyatkovskiĭ, Izv. Ross. Akad. Nauk, Ser. Fiz. **64**, 1060 (2000).
19. W. P. Mason and B. T. Matthias, Phys. Rev. **74**, 1622 (1948).
20. C. Perrin, N. Menguy, E. Suard, et al., J. Phys.: Condens. Matter **12**, 7523 (2000).
21. A. I. Fedoseev, S. G. Lushnikov, J.-H. Ko, and S. Kojima, Ferroelectrics **320**, 75 (2005).
22. P. Groves, J. Phys. C: Solid State Phys. **18**, L1073 (1985).
23. F. Chu, I. M. Reaney, and N. Setter, J. Appl. Phys. **77**, 1671 (1995).

Translated by P. Pozdeev